AGU PUBLICATIONS

JGR

Journal of Geophysical Research: Oceans

RESEARCH ARTICLE

10.1002/2015JC011365

Special Section:
Physical Processes Responsible for Material Transport in the Gulf of Mexico for Oil Spill Applications

Propagation of uncertainty and sensitivity analysis in an integral oil-gas plume model

Shitao Wang[1], Mohamed Iskandarani[1], Ashwanth Srinivasan[2], W. Carlisle Thacker[3], Justin Winokur[4], and Omar M. Knio[5,6]

[1]Rosenstiel School of Marine and Atmospheric Science, University of Miami, Miami, Florida, USA, [2]Tendral LLC, Miami, Florida, USA, [3]Miami, FL, USA, [4]Sandia National Laboratories, Albuquerque, New Mexico, USA, [5]Department of Mechanical Engineering and Material Science, Duke University, Durham, North Carolina, USA, [6]Division of Computer, Electrical and Mathematical Science and Engineering, King Abdullah University of Science and Technology, Thuwal, Saudi Arabia

Abstract Polynomial Chaos expansions are used to analyze uncertainties in an integral oil-gas plume model simulating the *Deepwater Horizon* oil spill. The study focuses on six uncertain input parameters—two entrainment parameters, the gas to oil ratio, two parameters associated with the droplet-size distribution, and the flow rate—that impact the model's estimates of the plume's trap and peel heights, and of its various gas fluxes. The ranges of the uncertain inputs were determined by experimental data. Ensemble calculations were performed to construct polynomial chaos-based surrogates that describe the variations in the outputs due to variations in the uncertain inputs. The surrogates were then used to estimate reliably the statistics of the model outputs, and to perform an analysis of variance. Two experiments were performed to study the impacts of high and low flow rate uncertainties. The analysis shows that in the former case the flow rate is the largest contributor to output uncertainties, whereas in the latter case, with the uncertainty range constrained by aposteriori analyses, the flow rate's contribution becomes negligible. The trap and peel heights uncertainties are then mainly due to uncertainties in the 95% percentile of the droplet size and in the entrainment parameters.

Key Points:
- Uncertainties in trap and peel height are quantified via their probability density functions
- The dominant contributors to output uncertainties are identified via analysis of variance
- When the flow rate uncertainty is constrained, the droplet size dominates the output uncertainties

Correspondence to:
S. Wang,
swang@rsmas.miami.edu

Citation:
Wang, S., M. Iskandarani, A. Srinivasan, W. C. Thacker, J. Winokur, and O. M. Knio (2016), Propagation of uncertainty and sensitivity analysis in an integral oil-gas plume model, *J. Geophys. Res. Oceans*, *121*, 3488–3501, doi:10.1002/2015JC011365.

Received 1 OCT 2015
Accepted 25 APR 2016
Accepted article online 24 MAY 2016
Published online 27 MAY 2016

1. Introduction

Multiphase plume modeling has a variety of environmental applications, such as the design of river plume outflows and sewage outfalls, reservoir destratification, [*Asaeda and Imberger*, 1993; *Lemckert and Imberger*, 1993; *Buscaglia et al*., 2002; *Sahoo and Luketina*, 2006; *Neto et al*., 2008], and guiding the response to accidental spills [*Johansen et al*., 2003; *Socolofsky et al*., 2011]. Great efforts have been spent in the models' development and validation. Reliable model predictions, however, require an additional step: uncertainties in model predictions caused by uncertainties in their input data must be quantified in order to gauge the confidence in the predictions, to identify the dominant contributors to their uncertainties, and to guide and prioritize the acquisition of additional data to reduce these uncertainties.

This study quantifies and analyses the uncertainties in a model simulating the near-field plume of the *Deepwater Horizon* (DWH) oil spill. The near-field is a region where turbulent mixing and various physical and chemical processes alter the plume's initial properties substantially, and sets the stage for the far-field evolution of the oil and gas spilled [*Gonçalves et al*., 2016]. The uncertain data considered here consist of empirical parameters needed to parameterize turbulent processes controlling the plume evolution, and the initial conditions of the flow near the well-head. More specifically, the uncertain inputs are: the oil flow rate at the well-head, the initial gas to oil ratio in the plume, two parameters controlling the droplet-size distribution, and two turbulent entrainment parameters. Section 2 provides more details on the model configurations and the choice of uncertain parameters. The uncertainties in these inputs were made more severe by the difficulty of conducting observations at the depth of ∼1500 m [*McNutt et al*., 2012] where the spill occurred, and by the uncertainties in the available information at the time of the estimate. The uncertainty analysis focuses on the following model outputs: the trap height which corresponds to the deepest intrusion layer where oil accumulates, the peel height where the plume's momentum vanishes, and the various gas mass fluxes.

Uncertainty Quantification (UQ) proceeds by first identifying the uncertain inputs and by specifying their distributions. Section 3 of the present article describes how a priori knowledge and observations were used

to specify the ranges of the uncertain input variables. The result is a parameter space whose dimension and size is determined by the number of uncertain variables retained, and by the uncertainty ranges selected, respectively.

Conventional approaches to UQ rely on Monte-Carlo (MC) sampling [*Homma and Saltelli*, 1996] to calculate the probability density function of the model outputs. A large number of model samples (with each sample corresponding to a different setting of the input variables) is required in order to obtain robust estimates of the output distributions. This approach becomes impractical [*O'Hagan*, 2006] when computational resources are limited, when the forward model is computationally expensive, when the dimension of the uncertainty space is large, and when rapid UQ analyses are needed for emergency response and quick decision support. The computational cost of the uncertainty analysis can be mitigated by seeking alternative sampling procedures and/or by minimizing the cost of a single sample. Both options are used in the present article.

The alternative sampling approach adopted here is based on nonintrusive Polynomial Chaos (PC) expansions [*Wiener*, 1938; *Ghanem and Spanos*, 1991; *Xiu and Karniadakis*, 2002; *Najm*, 2009; *Maître and Knio*, 2010], whereby a small ensemble of realizations is used to construct a faithful but cheap surrogate for the model. The surrogate is then used to calculate the statistical information required. The benefits of this approach are fourfold. First, the number of realization needed for the surrogate construction is much smaller than the one required by direct MC sampling. Second, a large sample can be generated at a much reduced cost using the surrogate instead of the actual model. Third, the technique can be used without changes to the forward plume model. Fourth, the surrogate is actually a polynomial series that can be easily manipulated and analyzed; in particular the analysis of variance, also referred to as global sensitivity analysis [*Crestaux et al*., 2009; *Alexanderian et al*., 2012], can be performed in a straightforward manner and without additional model samples. The PC approach has been successfully applied to quantify uncertainties in a variety of oceanic simulations [*Thacker et al*., 2012; *Winokur et al*., 2013; *Alexanderian et al*., 2012; *Iskandarani et al*., 2016].

The second cost mitigating step concerns the selection of the forward plume model. The simulation of near-field plumes in deep water oil spills is very challenging due to the turbulent, multiscale and multiphase (gas, oil, and water) nature of the flow, and would require long computational times on current supercomputers [*Fabregat et al*., 2015]. The model cost becomes an insurmountable hurdle when hundreds of model forecasts are required in a relatively short period of time to support emergency response and contingency planning. A compromise must then be struck between the model complexity and the details and fidelity with which it simulates the physical processes controlling the plume evolution. Here we opt to use an integral plume model as our forward model [*Asaeda and Imberger*, 1993; *Crounse et al*., 2007; *Socolofsky et al*., 2008]. The integral plume model achieves its efficiency by assuming a steady state and self-similar axisymmetric shape for the distribution of the plume properties, and by parameterizing the turbulent mixing processes between the plume and the surrounding fluid. The Navier-Stokes equations are then reduced to a set of nonlinear ordinary differential equations that are cheaper to solve than the original equations. Details of the mixing are lost and the focus is shifted to conservation of bulk quantities (such as mass, momentum, and energy). Fortunately, the long-term evolution of an oil-spill past the plume stage does not depend strongly on simulating the details of the mixing, but on estimating integral quantities, which can be simulated realistically with the integral plume model [*Asaeda and Imberger*, 1993; *Buscaglia et al*., 2002; *Johansen et al*., 2003].

Two classes of integral models have been developed to handle distinct flow regimes depending on the relative importance of ambient stratification and the background current. Descending outer plumes form and give rise to eventual intrusion layers [*Socolofsky et al*., 2008] at multiple depths when the background current is weak and stratification is present. The Texas A&M Oilspill Calculator (TAMOC) [*Crounse et al*., 2007; *Socolofsky et al*., 2008] is designed to handle this class of stratification-dominated regimes: it accounts for the presence of the double plumes and relies on an iterative algorithm to compute the mixing between the inner-outer plumes and the ambient fluid. The presence of a background flow suppresses the outer plumes, deflects the rising plume downstream, and gives rise to a substantial and forced entrainment between the plume and the current which must be accounted for. This type of plume regime is simulated using the Lagrangian integral model, such as the Comprehensive Deepwater Oil and Gas Blowout Model (CDOG) [*Chen and Yapa*, 2003] and the DeepBlow model [*Johansen*, 2003]. *Socolofsky et al*. [2015] provides a

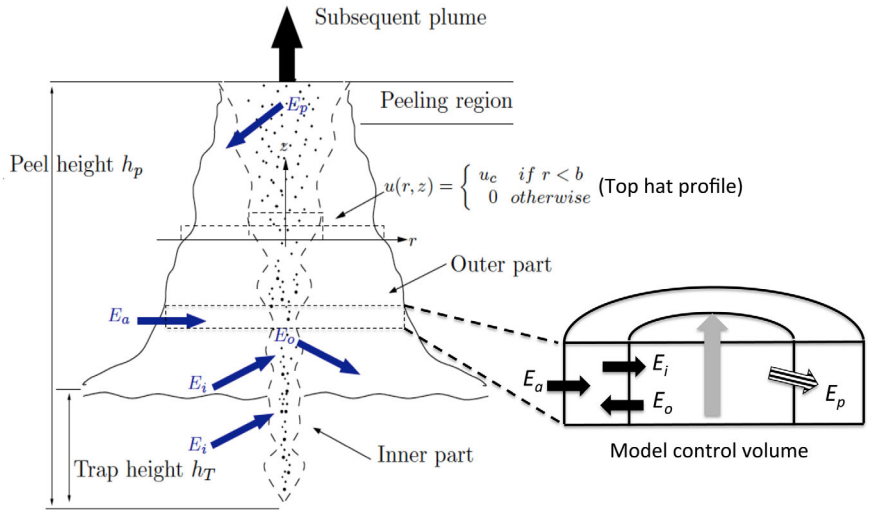

Figure 1. Schematic of buoyant plume dynamics in a stratified environment. Several variables are marked in the figure including the continuous phase velocity u, the constant velocity in top-hat profile u_c, the plume half width b, the vertical coordinate z, the radial coordinate r, the peeling flux E_p, and the entrainment fluxes E_a, E_i, E_o.

comprehensive intercomparison of different plume models. During the DWH oil spill, the deep currents near the well head were measured to be weak ($<$0.08 m/s) [*Camilli et al.*, 2010], and multiple intrusions were observed [*Socolofsky et al.*, 2011]. *Socolofsky et al.* [2011] concluded that the plume behavior was mainly controlled by the ambient stratification instead of cross flow during the DWH oil spill. Thus, we use the double plume integral model in our study.

The layout of this paper is as follows. Section 2 describes the physical processes in the near-field of an oil spill, and highlights the major features of the integral plume model. The uncertainty input parameters and the setup of the experiments are described in section 3. Section 4 introduces the PC construction and sensitivity analysis method. Section 5 provides the results of the uncertainty propagation and sensitivity analysis. Section 6 presents the summary and future work.

2. Model Description

Oil droplets and gas bubbles of different sizes and different chemical compositions are released into the environment during an oil spill. The near-field oil plume is thus a multiphase flow consisting of a continuous seawater phase and the dispersed phases of oil and gas. The primary processes controlling the near-field dynamics are: buoyancy forces acting on different phases, turbulent entrainment, buoyant peeling, and gas dissolution [*Crounse et al.*, 2007]. Figure 1 is a conceptual sketch of buoyant jet dynamics in a stratified environment. The "oil" escapes from the broken pipe as a mixture of oil droplets and gas bubbles whose buoyancy accelerates the ambient fluid to form an upward moving inner plume. Turbulent mixing at the plume edges entrains ambient fluid into it via an entrainment flux E_i causing the plume's buoyancy to decrease. Eventually the inner plume becomes negatively buoyant and decelerates due to the ambient stratification. When the momentum flux of the inner plume approaches zero at the so-called peel height h_P, the maximum height to which the inner plume rises, an annular ring outer plume forms and descends as a peeling flux E_p. Due to oil/gas buoyancy, some of the fluid remaining in the inner plume will continue rising as a subsequent plume. Turbulence around the descending outer plume generates two new entrainment fluxes: E_a from the ambient environment to the outer plume, and E_o from the inner plume to the outer plume. The descending outer plume will eventually be halted by the ambient stratification at the trap height h_T, which is a neutral buoyancy layer above the source where ambient density is equal to the outer plume's density.

TAMOC version 0.1.5 (https://github.com/socolofs) [*Socolofsky et al.*, 2008] is adopted as the forward model in the present numerical experiments. TAMOC's complete description can be found in *Crounse et al.* [2007] and *Socolofsky et al.* [2008]; here we give a brief overview of the model and refer the reader to the TAMOC manual for more details. TAMOC accounts for the near-field double plume dynamics in a stratification-

Table 1. Summary of DWH Release Conditions [*Lehr et al.*, 2010; *Valentine et al.*, 2010; *Reddy et al.*, 2012][a]

Parameters	Deepwater Horizon Values
Release depth	1500 m
Pressure	CTD(R/V Brooks McCall at Station B54)
Salinity	CTD(R/V Brooks McCall at Station B54)
Ambient temperature	CTD (R/V Brooks McCall at Station B54)
Gas and oil temperature	37°C
Diameter of riser	0.53 m
Oil density	858 kg/m^3
Oil gravity	40° API
Gas composition (mole fraction)	[methane, ethane, propane] [0.875, 0.081, 0.044]
Gas to oil ratio	
Flow rate	
Entrainment parameters	⇒ Uncertain parameters
Mass flux of oil of different droplet sizes	
Mass flux of gas of different bubble sizes	

[a]The chemical properties for each of the gas components are from the library in TAMOC.

dominated deepwater blowout, and for the presence of the continuous seawater phase, and the dispersed oil and gas phases, each endowed with their own fluid properties and droplet-size distributions when applicable. The dispersed phases simulated in TAMOC can be treated as either soluble or insoluble fluid particles with different predefined chemical compositions. TAMOC parameterizes the dispersed-phase mass transfer using a discrete bubble submodel [*Wüest et al.*, 1992] to model the dissolution process. Furthermore, the model has the capability to handle an arbitrary number of dispersed phases, each with its own sizes.

TAMOC solves a set of ordinary differential equations of the form

$$\frac{d\vec{Q}}{dz} = \vec{F}(\vec{X}, \vec{A}, z), \text{ with } \vec{Q}(z=0) = \vec{Q}_0 \quad (1)$$

where $\vec{Q}(z)$ represents the vector of conserved quantities (such as mass and momentum fluxes); $\vec{X}(z)$ represents the vector of plumes properties (such as their widths and vertical velocities), $\vec{A}(z)$ represents the vector of ambient variables (such as temperature and salinity); z denotes depth, $\vec{F}$ represents the flux exchanges among the inner plume, outer plume and the ambient fluid, or the exchanges among the different fluid phases; and $\vec{Q}_0$ represents the initial flux at the plume source. Equations (1) are supplemented with different equations of state, parameterizations, and closure schemes to close the system of equations. Once the release conditions $\vec{Q}_0$ and ambient conditions are specified, the plume properties $\vec{X}(z)$ can be computed by solving the set of equations (1).

Our application of TAMOC to the DWH oil spill uses observational data to specify the release conditions, including the release depth, the diameter of the release port, the temperature, and the detailed composition of the spilled oil and gas at the release (shown in Table 1). The environmental conditions for our experiments were obtained from a CTD profile from R/V Brooks McCall at Station B54 (28°43.945'N, 88°22.607'W; 30 May 2010). We use the two-parameter Rosin-Rammler distribution to model the range of oil/gas droplet sizes, which are then discretized into 20 distinct bins. We treat the two parameters of the Rosin-Rammler distribution as uncertain as explained in section 3.3. Three different equations of state are used here: the Peng-Robinson equation for the gas phase [*McCain*, 1990], the liquid specific gravity equation for the oil phase [*McCain*, 1990], and the seawater equation of *Gill* [1982] for the water phase. The oil flowrate and GOR are specified at standard conditions, and the gas is released as free gas (the equilibrium partitioning of the gas in the oil at depth is not considered). We treat both the GOR and the oil flow rate as uncertain inputs (sections 3.2 and 3.4). It should be noted that dead oil was used in our experiments with soluble compounds (e.g., methane, ethane, propane) released only in the gas phase while the oil phase contained only insoluble compounds (oil dissolution is negligible compared with that of gas) [*Yapa et al.*, 2012]. In a live oil release case, a significant fraction of soluble compounds dissolve into the oil phase, which leads to a lower flow rate for the gas phase and a lower density for the oil phase [*Socolofsky et al.*, 2015].

Trap height (h_T, Figure 1), peel height (h_P, Figure 1), and different gas mass fluxes are selected as our output quantities of interest. The trap height is defined as the level at which the momentum of the downward-moving outer plume becomes zero and the peel height is defined as the level at which the momentum of the upward-rising inner plume becomes zero. The methane, ethane and propane mass fluxes for the first 500 meters above the wellhead are constantly monitored because the gas dissolution process and the change of bubble size distribution are reflected in changes in the gas mass fluxes.

3. The Uncertain Input Parameters

A complete UQ analysis requires considering all sources of uncertainty, such as model parameters, initial conditions, and boundary conditions. The ensuing uncertain space would have a very large dimension and its exploration via ensemble runs would incur a huge computational burden. It is thus common to focus on the dominant sources of uncertainty. The uncertain parameters here are tightly related to the primary processes controlling the evolution of a multiphase plume in density stratified environments [*Crounse et al*., 2007]: buoyant forces acting upon the continuous phase and dispersed phases, dissolution of gas bubbles, entrainment, and peeling. Uncertainties in the ambient environment during the oil spill may also impact the plume behavior. However, a preliminary experiment showed that the uncertainties in the ambient environment (salinity, temperature, and pressure) are small compared to that of other parameters. Furthermore, the ambient environment in the deep ocean is relatively stable and easy to measure; we thus exclude the ambient environment uncertainties from our numerical experiments. The next step of UQ is to characterize the PDFs of the uncertain inputs. Unfortunately, the data from laboratory or field studies are insufficient to build a reliable PDF empirically. Therefore, we use available data to identify the ranges of the uncertain parameters and assume that their PDFs are uniformly distributed. Note that the model output uncertainties depend critically on the assumed distributions of input uncertainties as was discussed in *Thacker et al*. [2015]. However, the availability of a surrogate enables users to change the estimated output uncertainties by resampling the surrogate, no new model runs need to be performed. The following subsections discuss how measurements and theoretical arguments are used to specify the ranges of these uncertain inputs.

3.1. Entrainment Coefficient

The entrainment processes in the multiphase plume contribute to the injection of the negative buoyancy into the plume and therefore lead to the appearance of the double plume recirculation. TAMOC relies on several entrainment coefficients to parametrize the different turbulent entrainment processes. *Socolofsky et al*. [2008] pointed that an important uncertainty in the double plume model is the entrainment parameter between the inner and outer plumes. The uncertainties of the other entrainment parameters arise mainly because the multiphase plumes are not strictly self-similar as shown in laboratory studies by *Milgram* [1983] and *Seol et al*. [2007].

Although three entrainment parameters exist, the α_o (inner to outer) and α_a (ambient to outer) entrainment coefficients are found to be about equal experimentally [*Asaeda and Imberger*, 1993; *Seol et al*., 2007]; we are then left with only two independent parameters. *Bhaumik* [2005] studied the sensitivity of trap height and peel height to the entrainment coefficients of the plume model and compared the numerical model predictions with laboratory experiments. The entrainment coefficient α_a in his experiments was set to 0.06, 0.087, and 0.116 (top-hat profile is assumed here), and the ratio α_i/α_a was set to 0.25, 0.5, and 0.75 for different model runs. The experimental data did not show a clear advantage for the three values of α_a tested and, therefore, we adopt the lower and upper bounds as our uncertainty range. *Asaeda and Imberger* [1993]; *Bhaumik* [2005] found that $\frac{\alpha_i}{\alpha_a}=0.5$ gave the best comparison with experimental data. Since $\frac{\alpha_i}{\alpha_a}=0.4$ would correspond to a pure jet entrainment [*Asaeda and Imberger*, 1993], we, therefore, perturb $\frac{\alpha_i}{\alpha_a}$ by around 20% of its experimental best match value (0.4–0.6).

3.2. Gas to Oil Ratio

The amount of gas released by an oil spill is determined by the combination of gas to oil ratio (GOR) and oil flow rate. Deep ocean GOR measurements span a large range. *Reddy et al*. [2012] collected the compositional information for gas/oil mixture from two deep water samples which provided a GOR of 1600 and 2470 ft^3/barrel, respectively, while *Valentine et al*. [2010] used a GOR of 3000 ft^3/barrel in their studies. *McNutt et al*. [2012] suggested a GOR variation from 1400 to 2400 ft^3/barrel based on the linear trend of lower marine riser package. We adopt the lower and upper bound of the listed reference values as our uncertainty range for GOR.

3.3. Initial Gas/Oil Droplet Distribution

The droplet size is the main parameter affecting the rising speed and the dissolution rate for a given oil/gas composition and density. The two-parameter Rosin-Rammler distribution [*Lefebvre*, 1989] is used as initial oil droplet/gas bubble-size distribution because of its simplicity, its wide acceptance, and its agreement

Table 2. Uncertain Input Variables and Their Perturbation Ranges for the Flow Rate's High and Low Uncertainty Experiments[a]

Parameter	Variable	6D HUE	6D LUE
Entrainment coefficient [*Bhaumik*, 2005]	ξ_1	(0.06, 0.116)	(0.06, 0.116)
Entrainment ratio [*Bhaumik*, 2005]	ξ_2	(0.4, 0.6)	(0.4, 0.6)
Gas to oil ratio [*Reddy et al*., 2012; *Valentine et al*., 2010]	ξ_3	(1400, 3000)	(1400, 3000)
95th percentile of the droplet size (d_{95}) (mm) [*Johansen et al*., 2001, 2013]	ξ_4	(1, 10)	(1, 10)
Droplet distribution spreading ratio [*Lefebvre*, 1989]	ξ_5	(1.5, 4)	(1.5, 4)
Flow rate (barrels/day) [*McNutt et al*., 2012]	ξ_6	(5,000,60,000)	(50,000,70,000)

[a]The table also shows the standard random variable $-1 \leq \xi_i \leq 1$ corresponding to each physical parameter; the mapping between the physical and standard ranges is linear.

with the *Deepspill* experiment data [*Johansen et al*., 2013; *Brandvik et al*., 2013]. The volume contained in droplets with diameter larger than d can be expressed as:

$$V(d) = 1 - \exp\left[-2.996(d/d_{95})^n\right] \tag{2}$$

Here, d_{95} is the 95th percentile of the droplet size and n is a distributional spreading parameter. For most sprays, the value of n lies between 1.5 and 4 [*Lefebvre*, 1989].

Observations during the DWH provide little information about the released droplet sizes, and guidance can be sought from either droplet-size distribution models or observations from previous deepwater oil spills. The largest observed droplet size in the only deep water oil spill field experiment, DeepSpill [*Johansen et al*., 2003], is 10 mm. But differences between the DeepSill and DWH conditions prevent these observations from being used directly because of dissimilarities in the exit conditions and the oil breakup regime between the two spills (with the Weber number in the DWH being ten times larger than in DeepSill). *Johansen et al*. [2013] developed a correlation model to and scale their laboratory measurements to the field scale. Their analysis suggests that, without chemical dispersants, the expected droplet sizes in DWH were approximately in the range of 1–10 mm; whereas chemical dispersants can reduce the droplet size to the range of 100–1000 μm. However, the effectiveness of the chemical dispersants has recently been put into question by *North et al*. [2015], and they suggested that a wide range of droplet sizes is possible. *Zhao et al*. [2015] simulated the droplet size evolution as a function of depth during DWH using a dynamical population model (VDROP-J) [*Zhao et al*., 2014], and investigated the effects of different initial sizes, ranging from 1 to 10 mm, on the simulation results. Here, we adopt the largest range for d_{95}, namely 1–10 mm, to cover the widest possible range.

3.4. Flow Rate

The flow rate was, perhaps, one of the most important unknowns in the *Deepwater Horizon* oil spill. A flow rate estimation was conducted at the very beginning of the oil spill. On 28 April, NOAA released the first official flow rate of the *Deepwater Horizon* oil spill as 5000 barrels/day [*Guard*, 2011]. This flow rate was estimated from satellite images, which is highly inaccurate without additional in situ information. On 12 May, many researchers suggested that the flow rate was much higher than 5000 barrels/day based on the publically released videos of the damaged riser. Based on in situ measurements and numerical simulations, *McNutt et al*. [2012] suggested a flow rate in the range of 50,000–70,000 barrels/day. The initial flow rate estimate differs from the final one reported by *McNutt et al*. [2012] by a factor of 10. *Socolofsky et al*. [2011] showed that some plume properties (e.g., trap height) only depend on the flow rate to the 1/4-power, and thus, theoretically, we do not expect the flow rate uncertainty to dominate the uncertainty in the model output. We propose two different experiments to represent two different uncertainty scenarios that a user might contemplate (shown in Table 2): one scenario accounts for the aposteriori information available regarding the spill, and another scenario reflects the a priori lack of reliable information on the flow rate at the time of the estimate.

In the Low Uncertainty Experiment (LUE), we perturb the flow rate around its final estimate (between 50,000 barrels/day and 70,000 barrels/day). In the High Uncertainty Experiment (HUE), we perturb the flow rate using a large range (between 5000 barrels/day and 60,000 barrels/day). This two-experiment setup illustrates the impacts of specifying the ranges of the uncertain inputs on the statistical analysis of the model outputs.

4. Methodology

A PC expansion is a spectral-type series [*Maître and Knio*, 2010] that describes the dependence of the model output on the uncertain variables:

$$u(z,\xi) \approx u_P(z,\xi) = \sum_{n=0}^{P} \hat{u}_n(z)\psi_n(\xi) \tag{3}$$

Here $u(z,\xi)$ is a model output and u_P is its truncated series representation (essentially the surrogate); $\hat{u}_n(z)$ are the PC coefficients; z is the vertical coordinate from the wellhead; $\xi = (\xi_1, \ldots, \xi_6)^\top$ is the vector of stochastic variables encapsulating the uncertainty in the input parameters with PDF $p(\boldsymbol{\xi_i})$; and $\psi_n(\xi)$ are basis functions in the ξ-space. The correspondence between the standard variables ξ_i and the physical parameters is listed in table 2. Here, the basis functions are multidimensional orthogonal Legendre polynomials as we assume the parameters to be uniformly distributed [*Maître and Knio*, 2010; *Xiu and Karniadakis*, 2002]. Again, the model output uncertainties depend on the specified PDF of the input uncertainties. For convenience and lack of more specific information, we use the simple uniform distribution.

Two issues arise when constructing a PC surrogate, namely selecting the series truncation P and determining the PC coefficients. These choices depend on the nature of the model response to the varied model inputs. A closer inspection of the 1d response curves shows that the output of the model is noisy. This noise may be due to the sensitivity of the model to both the measured CTD profile and the variation of the input parameters; as the state variables are integrated in depth, small changes may amplify the noise in the model outputs. This noise is negligible from a practical point of view. The large-scale trends are smooth and can be represented with low degree polynomials. The oscillations, on the other hand, have a small amplitude and scale and would require a very long series to be approximated. To avoid overfitting the model noise, we use a polynomial basis of maximum degree 5 to capture the trends. The traditional multidimensional PC representation uses a total degree truncation so that mixed-order terms with total degree larger than 5 are dropped from the PC representation (the series contains 462 polynomials and $P = 461$). The Basis Pursuit Denoising (BPDN) algorithm, a type of compressive sensing technique, is adopted to calculate the PC coefficients because it is robust against noisy model outputs, and because it enforces a sparse representation (alternate approaches are discussed in *Iskandarani et al*. [2016]). The number of PC coefficients is 462, and an empirical rule of thumb calls for an ensemble size one-half to one-third the number of coefficients, roughly 200 samples. The 200 member ensemble is generated using a Latin hypercube sampling method. Once the ensemble is available, the coefficients can be computed with the help of the Matlab solver SPGL1 [*Van Den Berg and Friedlander*, 2007]. It is worth pointing out that the solver requires a value for the noise level to avoid overfitting; this noise level was determined by a cross-validation procedure as proposed in *Doostan and Owhadi* [2011] and *Peng et al*. [2014].

Global sensitivity analysis, or the analysis of variance, aims to quantify the contributions of each parameter to the variance of the model output. First-order sensitivity indices S and total sensitivity indices T are used to quantify the influence of uncertain inputs on the quantities of interest. Specifically, S describes the effect of individual parameters only on the model output without any interactions with others; while T measures the "total effect" of a specific parameter which accounts for the variability due to its individual influence and all its possible interactions with other parameters. These two sensitivity measures can be easily obtained from the PC coefficients as follows:

$$S_i = \frac{\sum_{\alpha \in \mathbb{S}_1^i} \hat{u}_\alpha^2 < \Psi_\alpha, \Psi_\alpha >}{V_{total}} \tag{4}$$

$$T_i = \frac{\sum_{\alpha \in \mathbb{S}_T^i} \hat{u}_\alpha^2 < \Psi_\alpha, \Psi_\alpha >}{V_{total}} \tag{5}$$

where $\mathbb{S}_1^i$ denotes the index set of all monomial terms of ξ_i and $\mathbb{S}_T^i$ denotes the index set of all polynomials including ξ_i. V_{total} is the total variance. For more information, the reader is referred to *Homma and Saltelli* [1996]; *Sobol* [2001]; *Crestaux et al*. [2009]; *Alexanderian et al*. [2012].

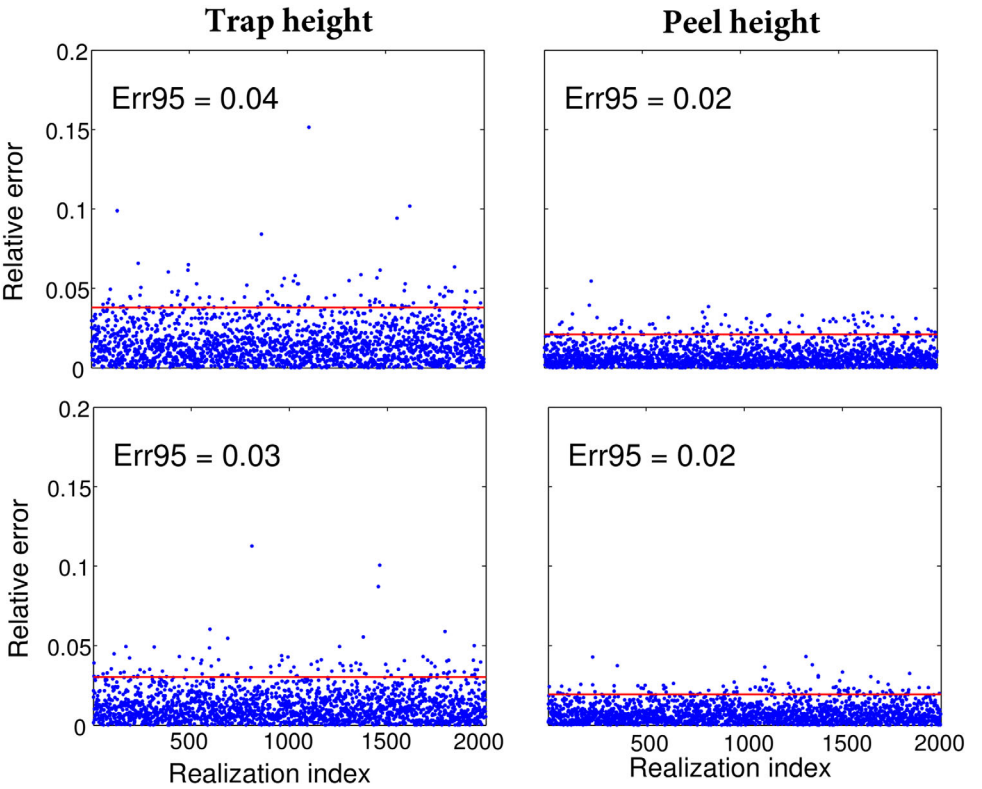

Figure 2. (left) Relative approximation error and Err95 for trap height and (right) peel height in (top) HUE and (bottom) LUE.

5. Results

5.1. Error Metrics

Two independent ensembles, generated by Latin hypercube sampling, were produced for the uncertainty analysis. One ensemble, consisting of 200 samples, was used in the construction of the surrogate; the other, consisting of 2000 samples, was calculated to validate the approximation errors incurred by the surrogate. The relative approximation error is defined as:

$$\epsilon(\xi_i^v) = \frac{|u_P(\xi_i^v) - u(\xi_i^v)|}{\max(u) - \min(u)}, \quad i = 1, 2, \ldots, 2000 \tag{6}$$

where ξ_i^v denotes one of the validation samples, $u_P(\xi_i^v)$ denotes the surrogate evaluated at the i-th validation sample, and $u(\xi_i^v)$ the directly sampled response at the same validation point. A statistical error measure, namely the 95th percentile level of the local relative error, which we refer to as Err95, is adopted to gauge the quality of the approximation error.

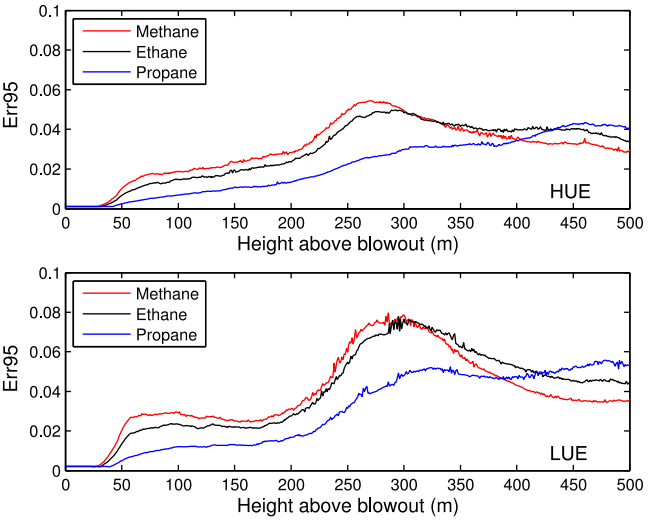

Figure 3. Err95 for methane, ethane, and propane gas mass fluxes in (top) HUE and (bottom) LUE.

Figure 2 depicts the scatter plots of the relative local error along with its Err95 for trap height and peel height in both experiments. The Err95 are

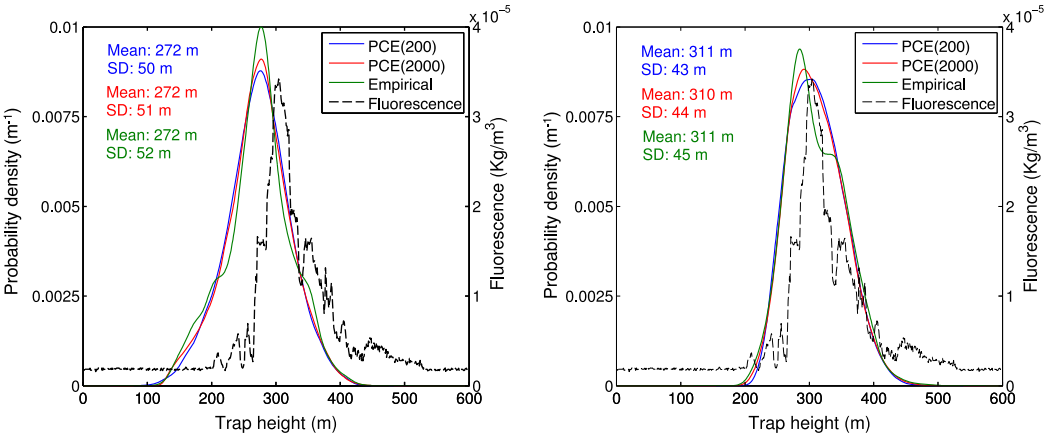

Figure 4. Comparison of trap height PDFs and the fluorescence measurement for (left) HUE and (right) LUE. Within each plot, the left *y* axis is the probability density and the right *y* axis is fluorescence intensity. The blue solid curve represents the trap height PDF estimated from PC expansion built with a 200 member ensemble (fifth-degree PC basis). The red solid curve depicts the trap height PDF estimated from PC expansion built with a 2000 member ensemble (ninth-degree PC basis). Again, these PDFs are obtained by sampling the PC surrogate 100,000 times. The green solid curve is the empirical trap height PDF estimated directly from the 2000 member ensemble. The mean and standard deviation (SD) of each PDF are color-coded accordingly. The black dash curve is the fluorescence measurement.

0.04 and 0.03 for trap height in HUE and LUE, respectively, while the Err95 for peel height are both 0.02. Figure 3 shows the Err95 for different gas mass fluxes as a function of depth. The peak of the Err95 is approximately 0.05 in HUE and 0.07 in LUE. The average Err95 for all gases is about 0.05 over the first 500 m. The error analysis thus suggests that the PC surrogates have low relative error levels, and provide adequate accuracy for the uncertainty analysis.

5.2. Trap and Peel Height Statistics

The PDFs of the quantities of interest reflect the influence of all input uncertainties, and can be obtained efficiently by analyzing 100,000 randomly generated samples using the PC surrogate. Furthermore, in order to investigate the reliability of the trap and peel height PDFs and get the most from the existing model realizations, three different PDFs are calculated and compared (Figures 4 and 5). Two of these PDFs are obtained using two differently constructed PC surrogates: one is built using the 200 member ensemble and a fifth-degree PC surrogate; the other is built with a 2000 member ensemble using a ninth-degree PC

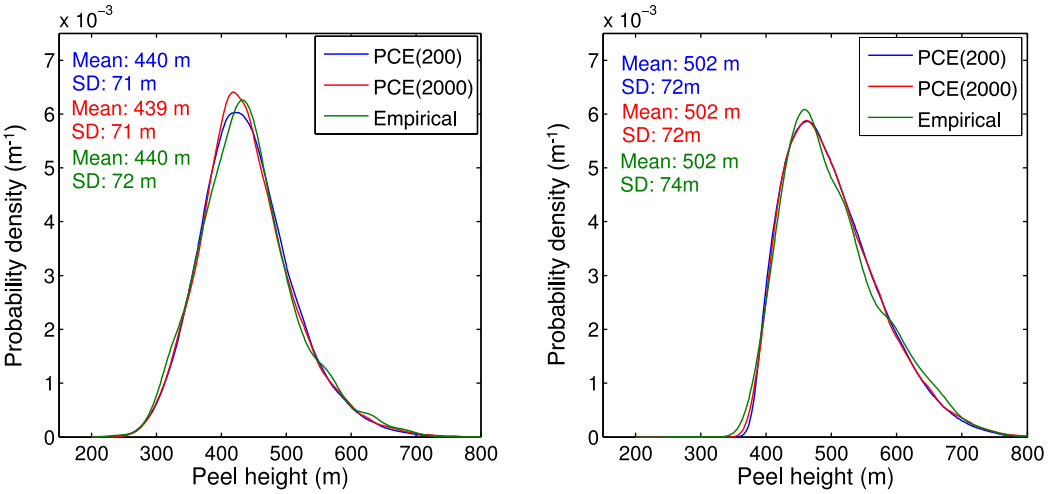

Figure 5. Comparison of different peel height PDFs. The blue solid curve represents the peel height PDF estimated from PC expansion built with a 200 member ensemble (fifth-degree PC basis). The red solid curve depicts the peel height PDF estimated from PC expansion built with a 2000 member ensemble (ninth-degree PC basis). Again, these PDFs are obtained by sampling the PC surrogate 100,000 times. The green solid curve is the empirical peel height PDF estimated directly from the 2000 member ensemble. The mean and standard deviation (SD) of each PDF are color-coded accordingly.

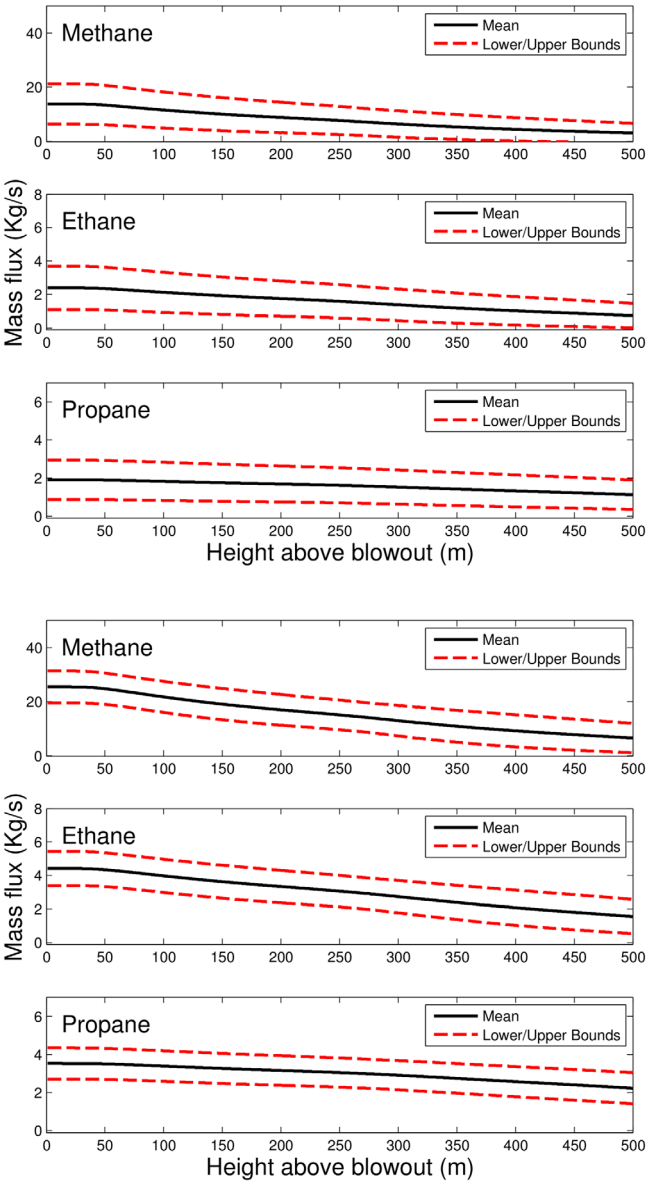

Figure 6. Mean and standard deviation of gas mass fluxes associated different gas components (methane, ethane, and propane) for the first 500 meters of blowout. (top) HUE; and (bottom) LUE.

surrogate. A third PDF is built directly from the 2000 member validation ensemble which we refer to as an empirical PDF. In HUE, the three trap height PDFs are in agreement, lead to very similar statistical moments as shown in Figure 4, and differ slightly in their estimate of the mode's probability; furthermore the output uncertainty ranges from 100 to 400 meters with a mode at about 275 m, mean of 272 m and standard deviation of 51 m. For LUE the trap height uncertainty range is now 200–425 m, and the mean and standard deviation are about 311 m and 44 m for all three estimates of the PDFs. The main difference among the different LUE trap height PDFs concerns the mode of the distribution which shifts slightly to lower values for the 2000 member PC surrogate and for the empirical PDFs; furthermore, the empirical PDF exhibits a slight shoulder that is missing from the PC-estimated trap height PDFs. Generally, the three LUE trap height PDFs agree with each other over most of the trap height uncertainty range.

Figure 5 shows the three estimates of the peel height PDFs for both experiments. The three estimates are basically in agreement for each case with slight differences near the mode of the PDF for the HUE. The PDFs from the PC surrogates overlap each other for much of the peel height uncertainty range in LUE. The statistical moments delivered by the three estimates are almost identical in both experiments. The major difference is in comparing the HUE and LUE PDFs. The former shows a mean peel height of 440 m while the latter shows a mean of 502 m. Interestingly the standard deviation in both experiments is the same, about 72 m, indicating that the uncertainty in the peel height did not improve with a smaller uncertainty range for the flow rate. This is likely due to the uncertainty in other parameters, most likely d_{95}, which now dominates the contribution to the peel height uncertainty; this is hinted by the sensitivity analysis shown below in section 5.4.

The estimated trap height PDFs are compared with observations collected during the *Deepwater Horizon* oil spill in Figure 4. The trap height can be identified as a level of oil accumulation and approximated by the oil concentration maximum, but no direct measurement is available. Fortunately, CTD fluorescence intensity measurement can be considered as a proxy for oil concentration [*Socolofsky et al.*, 2011]. The fluorescence intensity was obtained from the CTD cast of the R/V Brooks McCall at Station BM54 on 30 May 2010. Figure 4 indicates that the fluorescence measurements peak coincides with, or is very close to, the mode of the trap height PDFs for the LUE experiment. The mode of the trap height in HUE is, however, lower than the

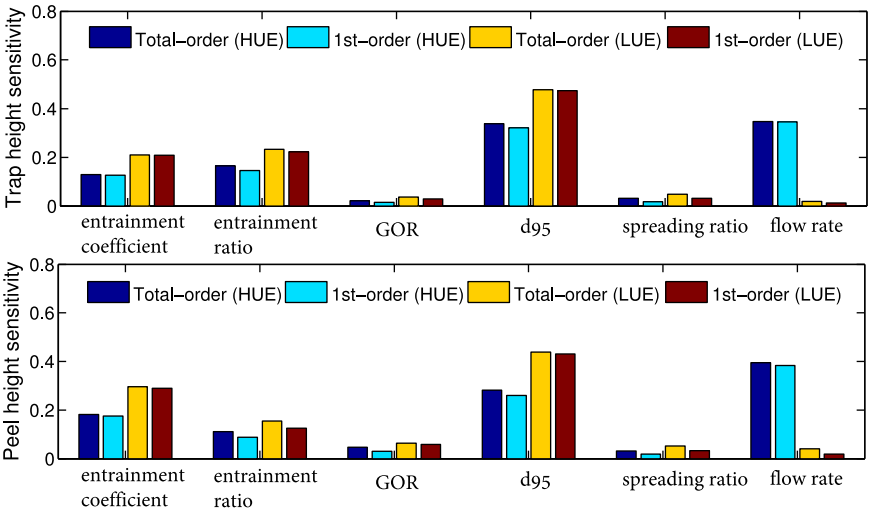

Figure 7. First and total-order sensitivity indices for (top) trap height and (bottom) peel height in HUE and LUE.

one inferred by observations; it nevertheless falls within the probable values. The standard deviations of the estimated trap height PDF in both experiments are similar which suggests that the trap height standard deviation is not sensitive to the perturbation range of the flow rate. The qualitative agreement between the LUE estimated predictions and observations confirm that the former's uncertainty range, 50,000–70,000 barrels/day, is more consistent with observations than the range of the HUE experiment.

5.3. Gas Mass Fluxes

The mean and standard deviation of the methane, ethane, and propane mass fluxes for the first 500 m above the wellhead are shown in Figure 6. The graphs show that a large amount of gases dissolve as the plume rises. With a methane to natural gas ratio of 0.875 [*Valentine et al*., 2010], about 50% (mean) of methane dissolves when the plume reaches the trap height (whose mode is around 250–300 m) in LUE and HUE. The observed fast dissolution of methane is consistent with many studies [*Valentine et al*., 2010; *Yvon-Lewis et al*., 2011; *Ryerson et al*., 2011; *Kessler et al*., 2011; *Ryerson et al*., 2012]: the majority of methane released from the wellhead was not reaching the surface during the *Deepwater Horizon* oil spill. The remaining gas mass fluxes at the trap height level indicate the importance of including gas into the far-field model for oil fate prediction. The flow rate perturbation leads to a substantial difference in the resulting methane mass flux statistics. In HUE, the methane mean mass flux starts at 13.8 kg/s at the wellhead and ends at 3.1 kg/s at 500 m away from the wellhead. In LUE, the methane mean mass flux starts at 25.5 kg/s at the wellhead and ends at 6.5 kg/s at 500 m away from the wellhead. The estimated standard deviation of methane mass flux also differs in these two experiments. Specifically, the estimated standard deviation decreases from 7.5 to 3.6 kg/s as the plume rises in HUE, while the standard deviation varies little, between 5.4 and 5.9 kg/s, as the plume rises in LUE.

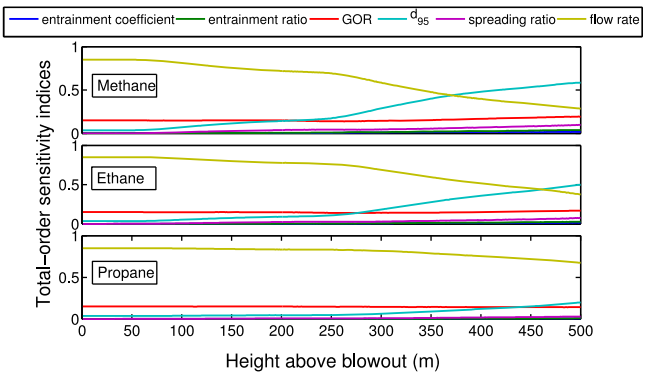

Figure 8. Evolution of the total sensitivity indices for methane, ethane, and propane gas mass fluxes associated with different uncertain input variables in HUE.

5.4. Sensitivity Analysis

Figure 7 shows the first-order and total-order sensitivity indices for trap height and peel height associated with different uncertain inputs. According to the sensitivity indices in HUE, the largest contributors to trap and peel height uncertainties are the flow rate and d_{95} in equal proportions, followed by the two entrainment parameters

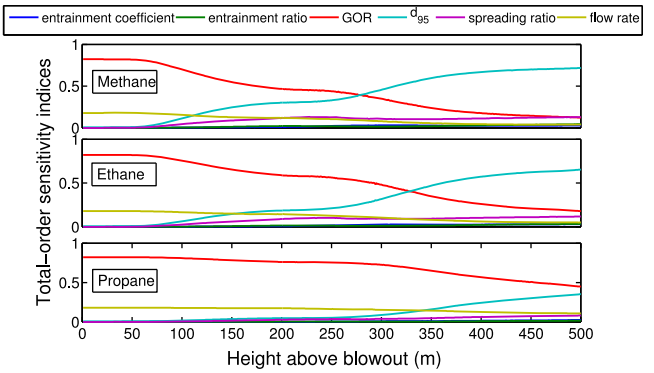

Figure 9. Evolution of the total sensitivity indices for methane, ethane, and propane gas mass fluxes associated with different uncertain input variables in LUE.

also in roughly equal proportions; the GOR and the spreading parameter, on the other hand, contribute little. In LUE, the sensitivity indices show that, the flow rate uncertainty stops being the dominant contributor to uncertainties in trap and peel heights once its range is narrowed. The d_{95} parameters exhibits then the highest sensitivity indices followed by the entrainment parameters. The results here suggest that narrowing the uncertainties in the flow rate and in the largest droplet size has a higher impact than that in the GOR and the spreading parameter.

The difference between the first-order and the total-order sensitivity indices can be considered as a measure of the interactions among different uncertain inputs, and whether the combined uncertainties magnify the output uncertainties. The results in Figure 7 point to weak interactions or couplings among different uncertain inputs as the first-order sensitivity indices are close to the total-order sensitivity indices.

The global sensitivity indices for methane, ethane, and propane mass fluxes as a function of depth are depicted in Figures 8 and 9. A basic observation from these results is that as the plume rises, d_{95} becomes clearly dominant in all cases. In HUE, the flow rate uncertainty is dominant at the initial stage, but its impacts on the total variance of different gas mass fluxes decreases as the plume rises. The flow rate sensitivity indices of methane mass flux decrease faster than those of ethane and propane. Additionally, propane sensitivity indices have the slowest decrease rate. In LUE, GOR is dominant at the initial stage and the uncertainty in d_{95} clearly prevails as the plume rises. This transition of the dominant parameter occurs at different distances from the wellhead for different gases: the transition for methane is around 270 m, the transition for ethane is around 330 m and the transition for propane is around 500 m.

6. Summary

This paper has analyzed the uncertainties in an integral plume model simulating the *Deepwater Horizon* oil spill using Polynomial Chaos surrogates. The study quantified the impacts of uncertainties in six input parameters on the model's estimates of the trap and peel heights, and the gas mass fluxes. The input uncertainties were primarily caused by missing data, and the available information about the input variables was used to define reasonable uncertainty ranges for the parameters. The major computational challenges during the surrogate construction were the sampling of a large six-dimensional parameter space, and handling the model noise. Both problems were successfully addressed using BPDN to calculate the PC coefficients using only 200 model samples. Various error metrics suggest that the PC surrogate is able to predict the response surface and the statistical information with acceptable fidelity.

The PC surrogates were used to estimate the PDFs of the different model outputs. Comparisons with fluorescence observations, a proxy for the oil accumulation at the trap height, show the observations coinciding with the mode of the trap height PDF for the LUE, thus suggesting that the latter range to be quite consistent with the fluorescence observations. The HUE case showed a lower probability of occurrence for the observations. Additionally, the natural gases do not dissolve completely at the trap height under any scenario, and therefore, the next stage numerical models must be able to handle this mixture of oil and gas in order to simulate the oil fate realistically. The sensitivity analysis of the trap height, peel height, and gas mass fluxes, indicates that the huge uncertainty range for the flow rate leads to substantial uncertainties in the ensuing quantities of interest whereas constraining the range to reasonable values shifts the dominance to the uncertainty in the largest droplet size and to uncertainties in the entrainment coefficients.

The present investigation suggests that the model outputs are insensitive to uncertainties in the flow rate provided it is known reasonably accurately. It also suggests that the next priority in observation should be aimed at estimating the largest droplet size and GOR if improvements in mass gas flux estimates are

desired, whereas the priority would fall on measuring the largest droplet size and the entrainment parameters if improvement in trap and peel heights is desired. If direct observations of these quantities prove to be difficult, then the collection of alternate data can still be useful as it can be used in an inverse uncertainty propagation exercise [*Sraj et al*., 2013] to correct the PDF of the model's *input* parameters. Likewise, if observations prove to be difficult or impractical, an additional compromise can be made, such as resorting to simulated data from very high-resolution numerical simulations [*Fabregat et al*., 2015].

Acknowledgments
We thank the two anonymous reviewers for their constructive suggestions which improve this manuscript. This work was made possible in part by a grant from BP/The Gulf of Mexico Research Initiative, and by the Office of Naval Research, Award N00014-101-0498. J. Winokur and O. M. Knio were also supported in part by the U.S. Department of Energy (DOE), Office of Science, Office of Advanced Scientific Computing Research, under Award DE-SC0008789. This research was conducted in collaboration with and using the resources of the University of Miami Center for Computational Science. The model data are publicly available in the Gulf of Mexico Research Initiative Information and Data Cooperative (GRIIDC) repository (https://data.gulfresearchinitiative.org/data/R4.x265.252:0002/).

References

Alexanderian, A., J. Winokur, I. Sraj, A. Srinivasan, M. Iskandarani, W. C. Thacker, and O. M. Knio (2012), Global sensitivity analysis in an ocean general circulation model: A sparse spectral projection approach, *Comput. Geosci.*, *16*(3), 757–778.

Asaeda, T., and J. Imberger (1993), Structure of bubble plumes in linearly stratified environments, *J. Fluid Mech.*, *249*, 35–57.

Bhaumik, T. (2005), *Numerical modeling of multiphase plumes: A comparative study between two-fluid and mixed-fluid integral models*, Master's thesis, A&M Univ., Tex. [Available at http://hdl.handle.net/1969.1/2607.]

Brandvik, P. J., Ø. Johansen, F. Leirvik, U. Farooq, and P. S. Daling (2013), Droplet breakup in subsurface oil releases–part 1: Experimental study of droplet breakup and effectiveness of dispersant injection, *Mar. Pollut. Bull.*, *73*(1), 319–326.

Buscaglia, G. C., F. A. Bombardelli, and M. H. García (2002), Numerical modeling of large-scale bubble plumes accounting for mass transfer effects, *Int. J. Multiphase Flow*, *28*(11), 1763–1785.

Camilli, R., C. M. Reddy, D. R. Yoerger, B. a. S. Van Mooy, M. V. Jakuba, J. C. Kinsey, C. P. McIntyre, S. P. Sylva, and J. V. Maloney (2010), Tracking hydrocarbon plume transport and biodegradation at Deepwater Horizon, *Science*, *330*(6001), 201–204, doi:10.1126/science.1195223.

Chen, F., and P. D. Yapa (2003), A model for simulating deep water oil and gas blowouts-part ii: Comparison of numerical simulations with deepspill field experiments, *J. Hydraul. Res.*, *41*(4), 353–365.

Crestaux, T., O. Le Maître, and J.-M. Martinez (2009), Polynomial chaos expansion for sensitivity analysis, *Reliab. Eng. Syst. Safety*, *94*(7), 1161–1172.

Crounse, B., E. Wannamaker, and E. Adams (2007), Integral model of a multiphase plume in quiescent stratification, *J. Hydraul. Eng.*, *133*(1), 70–76.

Doostan, A., and H. Owhadi (2011), A non-adapted sparse approximation of PDEs with stochastic inputs, *J. Comput. Phys.*, *230*(8), 3015–3034.

Fabregat, A., W. K. Dewar, T. M. Özgökmen, A. C. Poje, and N. Wienders (2015), Numerical simulations of turbulent thermal, bubble and hybrid plumes, *Ocean Modell.*, *90*, 16–28.

Ghanem, R. G., and P. D. Spanos (1991), *Stochastic Finite Elements: A Spectral Approach*, vol. 41, Springer, N. Y.

Gill, A. E. (1982), *Atmosphere-Ocean Dynamics*, vol. 30, Academic, San Diego, Calif.

Gonçalves, R. C., M. Iskandarani, A. Srinivasan, W. C. Thacker, E. Chassignet, and O. M. Knio (2016), A framework to quantify uncertainty in simulations of oil transport in the ocean, *J. Geophys. Res. Oceans*, *121*, doi:10.1002/2015JC011311.

Homma, T., and A. Saltelli (1996), Importance measures in global sensitivity analysis of nonlinear models, *Reliab. Eng. Syst. Safety*, *52*(1), 1–17.

Iskandarani, M., S. Wang, A. Srinivasan, W. C. Thacker, J. Winokur, and O. M. Knio (2016), An overview of uncertainty quantification techniques with application to oceanic and oil-spill simulations, *J. Geophys. Res. Oceans*, *121*, doi:10.1002/2015JC011366.

Johansen, Ø. (2003), Development and verification of deep-water blowout models, *Mar. Pollut. Bull.*, *47*(9), 360–368.

Johansen, Ø., H. Rye, A. Melbye, H. Jensen, B. Serigstad, and T. Knutsen (2001), Deep spill jip experimental discharges of gas and oil at helland hansen, *SINTEF Rep. 5TF66F01082*, pp. 1–159, SINTEF Appl. Chem., Trondheim, Norway

Johansen, Ø., H. Rye, and C. Cooper (2003), Deepspill-field study of a simulated oil and gas blowout in deep water, *Spill Sci. Technol. Bull.*, *8*(5), 433–443.

Johansen, Ø., P. J. Brandvik, and U. Farooq (2013), Droplet breakup in subsea oil releases–part 2: Predictions of droplet size distributions with and without injection of chemical dispersants, *Mar. Pollut. Bull.*, *73*(1), 327–335.

Kessler, J. D., et al. (2011), A persistent oxygen anomaly reveals the fate of spilled methane in the deep gulf of Mexico, *Science*, *331*(6015), 312–315.

Lefebvre, A. H. (1989), *Atomization and Sprays*, Hemisphere Publishing, N. Y.

Lehr, B., S. Bristol, and A. Possolo (2010), *Oil Budget Calculator, Deepwater Horizon*, 217 pp., Washington, D. C.

Lemckert, C. J., and J. Imberger (1993), Energetic bubble plumes in arbitrary stratification, *J. Hydraul. Eng.*, *119*(6), 680–703.

Le Maître, O. P., and O. Knio (2010), *Spectral Methods for Uncertainty Quantification: With Applications to Computational Fluid Dynamics*, Springer, N. Y.

McCain, W. D. (1990), *The Properties of Petroleum Fluids*, Penn Well Books, Tulsa, Okla.

McNutt, M. K., R. Camilli, T. J. Crone, G. D. Guthrie, P. A. Hsieh, T. B. Ryerson, O. Savas, and F. Shaffer (2012), Review of flow rate estimates of the deepwater horizon oil spill, *Proc. Natl. Acad. Sci. U. S. A.*, *109*(50), 20,260–20,267.

Milgram, J. (1983), Mean flow in round bubble plumes, *J. Fluid Mech.*, *133*, 345–376.

Najm, H. N. (2009), Uncertainty quantification and polynomial chaos techniques in computational fluid dynamics, *Annu. Rev. Fluid Mech.*, *41*, 35–52, doi:10.1146/annurev.fluid.010908.165248.

Neto, I. E., D. Z. Zhu, and N. Rajaratnam (2008), Air injection in water with different nozzles, *J. Environ. Eng.*, *134*(4), 283–294.

North, E. W., E. E. Adams, A. E. Thessen, Z. Schlag, R. He, S. A. Socolofsky, S. M. Masutani, and S. D. Peckham (2015), The influence of droplet size and biodegradation on the transport of subsurface oil droplets during the deepwater horizon spill: A model sensitivity study, *Environ. Res. Lett.*, *10*(2), 024016.

O'Hagan, A. (2006), Bayesian analysis of computer code outputs: A tutorial, *Reliab. Eng. Syst. Safety*, *91*(10), 1290–1300.

Peng, J., J. Hampton, and A. Doostan (2014), A weighted 1-minimization approach for sparse polynomial chaos expansions, *J. Comput. Phys.*, *267*, 92–111.

Reddy, C. M., et al. (2012), Composition and fate of gas and oil released to the water column during the deepwater horizon oil spill, *Proc. Natl. Acad. Sci. U. S. A.*, *109*(50), 20,229–20,234.

Ryerson, T., et al. (2011), Atmospheric emissions from the deepwater horizon spill constrain air-water partitioning, hydrocarbon fate, and leak rate, *Geophys. Res. Lett.*, *38*, L07803, doi:10.1029/2011GL046726.

Ryerson, T. B., et al. (2012), Chemical data quantify deepwater horizon hydrocarbon flow rate and environmental distribution, *Proc. Natl. Acad. Sci. U. S. A.*, *109*(50), 20,246–20,253.
Sahoo, G. B., and D. Luketina (2006), Response of a tropical reservoir to bubbler destratification, *J. Environ. Eng.*, *132*(7), 736–746.
Seol, D.-G., T. Bhaumik, C. Bergmann, and S. A. Socolofsky (2007), Particle image velocimetry measurements of the mean flow characteristics in a bubble plume, *J. Eng. Mech.*, *133*(6), 665–676.
Sobol, I. M. (2001), Global sensitivity indices for nonlinear mathematical models and their Monte Carlo estimates, *Math. Comput. Simul.*, *55*(1), 271–280.
Socolofsky, S. A., T. Bhaumik, and D.-G. Seol (2008), Double-plume integral models for near-field mixing in multiphase plumes, *J. Hydraul. Eng.*, *134*(6), 772–783.
Socolofsky, S. A., E. E. Adams, and C. R. Sherwood (2011), Formation dynamics of subsurface hydrocarbon intrusions following the deepwater horizon blowout, *Geophys. Res. Lett.*, *38*, L09602, doi:10.1029/2011GL047174.
Socolofsky, S. A., et al. (2015), Intercomparison of oil spill prediction models for accidental blowout scenarios with and without subsea chemical dispersant injection, *Mar. Pollut. Bull.*, *96*(1), 110–126.
Sraj, I., M. Iskandarani, A. Srinivasan, W. C. Thacker, J. Winokur, A. Alexanderian, C.-Y. Lee, S. S. Chen, and O. M. Knio (2013), Bayesian Inference of drag parameters using AXBT data from typhoon Fanapi, *Mon. Weather Rev.*, *141*(7), 2347–2367, doi:10.1175/MWR-D-12-00228.1.
Thacker, W. C., A. Srinivasan, M. Iskandarani, O. M. Knio, and M. L. Hénaff (2012), Propagating boundary uncertainties using polynomial expansions, *Ocean Modell.*, *43*, 52–63.
Thacker, W. C., M. Iskandarani, R. C. Gonçalves, A. Srinivasan, and O. M. Knio (2015), Pragmatic aspects of uncertainty propagation: A conceptual review, *Ocean Modell.*, *95*, 25–36.
US Coast Guard (2011), BP Deepwater Horizon Oil Spill: Incident Specific Preparedness Review (ISPR), Final Report[J], Department of Homeland Security, Washington, D. C. [Available at http://www.uscg.mil/foia/docs/DWH/BPDWH.pdf., Accessed November, 2011.]
Valentine, D. L., et al. (2010), Propane respiration jump-starts microbial response to a deep oil spill, *Science*, *330*(6001), 208–211.
van den Berg, E., and M. P. Friedlander (2007), *SPGL1: A Solver For Large-Scale Sparse Reconstruction*, British Columbia, Canada. [Available at http://www.cs.ubc.ca/labs/scl/spgl1.]
Wiener, N. (1938), The homogeneous chaos, *Am. J. Math.*, *60*(4), 897–936.
Winokur, J., P. Conrad, I. Sraj, O. Knio, A. Srinivasan, W. C. Thacker, Y. Marzouk, and M. Iskandarani (2013), A priori testing of sparse adaptive polynomial chaos expansions using an ocean general circulation model database, *Comput. Geosci.*, *17*(6), 899–911.
Wüest, A., N. H. Brooks, and D. M. Imboden (1992), Bubble plume modeling for lake restoration, *Water Resour. Res.*, *28*(12), 3235–3250.
Xiu, D., and G. E. Karniadakis (2002), The Wiener–Askey polynomial chaos for stochastic differential equations, *SIAM J. Sci. Comput.*, *24*(2), 619–644.
Yapa, P. D., M. R. Wimalaratne, A. L. Dissanayake, and J. A. DeGraff (2012), How does oil and gas behave when released in deepwater?, *J. Hydro-environ. Res.*, *6*(4), 275–285.
Yvon-Lewis, S. A., L. Hu, and J. Kessler (2011), Methane flux to the atmosphere from the deepwater horizon oil disaster, *Geophys. Res. Lett.*, *38*, L01602, doi:10.1029/2010GL045928.
Zhao, L., M. C. Boufadel, S. A. Socolofsky, E. Adams, T. King, and K. Lee (2014), Evolution of droplets in subsea oil and gas blowouts: Development and validation of the numerical model vdrop-j, *Mar. Pollut. Bull.*, *83*(1), 58–69.
Zhao, L., M. C. Boufadel, E. Adams, S. A. Socolofsky, T. King, K. Lee, and T. Nedwed (2015), Simulation of scenarios of oil droplet formation from the deepwater horizon blowout, *Mar. Pollut. Bull.*, *101*(1), 304–319.